Multiscale modelling of solid tumour growth: the effect of collagen micromechanics

Peter A. Wijeratne · Vasileios Vavourakis · John H. Hipwell · Chrysovalantis Voutouri · Panagiotis Papageorgis · Triantafyllos Stylianopoulos · Andrew Evans · David J. Hawkes

Received: date / Accepted: date

Abstract Here we introduce a model of solid tumour growth coupled with a multiscale biomechanical description of the tumour microenvironment, which facilitates the explicit simulation of fibre-fibre and tumour-fibre interactions. We hypothesise that such a model, which provides a purely mechanical description of tumour-host interactions, can be used to explain experimental observations of the effect of collagen micromechanics on solid tumour growth. The model was specified to mouse tumour data and numerical simulations were performed. The multiscale model produced lower stresses than an equivalent continuum-like approach, due to a more realistic remodelling of the collagen microstructure. Furthermore, solid tumour growth was found to cause a passive mechanical realignment of fibres at the tumour boundary from a random to a circumferential orientation. This is in accordance with experimental observations, thus demonstrating that such a response can be explained as purely mechanical. Finally, peritumoural fibre network anisotropy was found to produce anisotropic tumour morphology. The dependency of tumour morphology on the peritumoural microstructure was reduced by adding a load-bearing non-collagenous component to the fibre network constitutive equation.

Keywords Tumour mechanics · Microenvironment · Fibre remodelling · Finite element analysis

P.A. Wijeratne, V. Vavourakis, J.H. Hipwell, D.J. Hawkes
Centre for Medical Image Computing, Department of Medical Physics and Bioengineering, Engineering Front Building, Malet Place, University College London, London, WC1E 6BT, UK
Tel.: +44-20-76790177
E-mail: p.wijeratne@ucl.ac.uk

C. Voutouri, P. Papageorgis, T. Stylianopoulos
Cancer Biophysics Laboratory, Department of Mechanical and Manufacturing Engineering, University of Cyprus, Nicosia, 1678, Cyprus

A. Evans
Ninewells Medical School, Dundee, DD1 9SY, UK

1 Introduction

The tumour microenvironment is now widely accepted as being an important factor in the development, progression and invasion of cancerous cells (Liotta and Kohn, 2001). Whilst historically the focus of cancer research has been on studying the relationship between intrinsic genomic properties and extrinsic chemical stimuli, observed epigenetic effects of force transmission between cells and their microenvironment have established the idea of a mechanical phenotype (Butcher et al, 2009); that is, a pathological dependence on cell and tissue biomechanical properties (Jain et al, 2014). This dependence is mediated by mechanochemical systems — such as transmembrane adhesion receptors (eg. integrins) and cytoskeletal networks — which translate mechanical cues from the microenvironment to the cell nucleus (Janmey, 1998) and are hence expressed variously as changes in shape (Yeung et al, 2005), motility (Pelham and Wang, 1997), proliferation (Paszek et al, 2005), differentiation (Discher et al, 2005) and apoptosis (Chen et al, 1997).

These processes occur at multiple length scales: from the tissue (macroscopic) to cell (microscopic) and molecular (nanoscopic). At the macroscopic scale, studies of the effects of solid stress (i.e. the stress of the solid components of the tumour) at the outer tumour boundary have shown that the mechanical interaction between cells and the extracellular matrix (ECM) plays

an important role in regulating cell proliferation (Helmlinger et al, 1997; Cheng et al, 2009). Furthermore, microstructural properties of the ECM — such as collagen fibre structure and density — have been implicated in cancerous growth and invasion (Provenzano et al, 2006). Specifically, the authors identified three principal fibre alignments with respect to the tumour boundary: random, parallel and perpendicular, which corresponded to tumour initiation, growth and invasion. This is an example of tumour mediated ECM remodelling, which has been associated with invasiveness by histopathologic analysis of human cancer cell lines (Conklin and Keely, 2012).

The physical mechanisms producing these mechanical phenotypes are currently unknown, thus motivating the development of a physiologically accurate mathematical model to compare with experimental data and hence identify the fundamental constituent processes. In particular, it is desirable to separate active from passive processes as they involve very different cell behaviour. The field of mathematical tumour growth modelling is vast (Byrne, 2010; Cristini and Lowengrub, 2010; Frieboes et al, 2011; Kam et al, 2012), from its origins in coupled integro-differential equations to more complex descriptions involving two or more interacting constituents (multiphase models), continuum, discrete and multiscale solid mechanics characterisation of multicellular tumour spheroids (mechanical models) and stochastic formulations of cell-cell and cell-ECM interactions (agent-based models), to highlight only the broader schools of thought.

Here we focus on mechanical models, based on the assumption that ECM remodelling is dependent on the material properties of the tumour and peritumoural stroma and their mechanical interaction. Furthermore, such models allow for the simulation of growth-induced solid stresses, which have an effect on cell proliferation (Helmlinger et al, 1997), apoptosis and vessel compression (Stylianopoulos et al, 2012). Motivated by these observations, (Netti et al, 2000) investigated the role of the ECM in interstitial fluid transport in tumours using a bi-phasic viscoelastic model. They found that collagen density influences the tissue resistance to macromolecular transport and hence drug efficacy. Based on the same observations, (Ambrosi and Mollica, 2004) proposed an elastic model of the tumour and agarose, with growth accommodated by a multiplicative decomposition of the deformation gradient. Through numerical simulations and assuming spherical symmetry, they qualitatively reproduced the experimental observations of radial displacement over time and investigated the effect of residual stress. The assumption of a linearly elastic material was dropped by (Kim et al, 2011), who developed a three-dimensional hypoelastic continuum model of tumour growth and qualitatively reproduced observations of anisotropic growth into a heterogeneous media.

To account for an extracellular fluid component, (Ambrosi and Preziosi, 2009) proposed a multiphase formulation of the tumour and its environment. This model was able to account for a number of complex interactions, such as stress-dependent growth, cell reorganisation and the formation of a capsule around the tumour boundary. The effects of residual and yield stresses were further examined in (Preziosi et al, 2010), where an elasto-visco-plastic model was employed to describe the dual nature of cellular aggregates: solid-like under small stress and liquid-like under large stress. A similar approach was utilised by (Stylianopoulos et al, 2013; Mpekris et al, 2015), who included a fluid component via Darcy's law and extended the formulation to account for residual tissue stresses. They found that growth-induced and externally applied stresses can affect cancer cell growth by compressing the cells and deforming blood vessels. In all these studies the focus has been on modelling the tumour itself.

To our knowledge, there are currently no models that account explicitly for microstructural components of the tumour microenvironment. This work focuses on developing a numerical methodology to simulate an avascular spherical tumour expanding into a collagen fibre network, which we use to gain insight into the relationship between tumour growth and peritumoural microstructure. The novelty lies in the coupling — rather than the individual components — of macroscopic tumour growth with the microscopic description of the ECM, and the numerical implementation. The hypothesis we aim to test is whether such a model, which has a purely mechanical description of tumour-host interactions, can be used to explain experimental observations of the effect of solid tumour growth on its microenvironment and vice versa.

Following the work of both (Chandran and Barocas, 2007) and (Stylianopoulos and Barocas, 2007), a three-dimensional structural characterisation of the collagen networks is employed, allowing for explicit calculations of fibre-fibre and tumour-fibre force exchange. The fibre scale is coupled with the tissue scale via the application of volume averaging theory, which casts macroscopic quantities in terms of their averaged microscopic properties. Following (Ambrosi and Mollica, 2002) and (Kim et al, 2011), tumour growth is incorporated through a multiplicative decomposition of the deformation gradient and driven by the concentration of oxygen. To motivate the multiscale approach, peritumoural collagen fibre network deformation and reorientation for affine

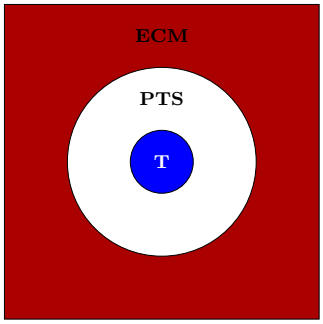

Fig. 1: Schematic representation of the analysed three-dimensional domain, from inside out: tumour (T), peritumoural stroma (PTS) and extracellular matrix (ECM).

and non-affine fibre kinematics are compared. In addition, experiments are performed to specify the model and determine parameter values. Details of the mathematical formulation, experimental procedure, numerical methodology and application are presented in the following sections.

2 Mathematical model

The cubic domain of interest is split into three subdomains: a sphere representing the tumour mass, an outer shell representing the peritumoural stroma (PTS), and a surrounding region representing the ECM. The tumour and ECM are treated as hyperelastic continua, while the PTS is represented by a multiscale (micro-macro) model of collagen networks. In principle all regions could be treated as multiscale but the focus of this analysis is mainly on the microstructural behaviour of the PTS.

2.1 Tumour growth

To model tumour growth, the deformation gradient, F_{ij}, is first decomposed into passive (elastic), F^p_{ik}, and growth (inelastic), F^g_{kj}, components: $F_{ij} = F^p_{ik}F^g_{kj}$ (Rodriguez et al, 1994). This can be thought of as a passive deformation operator which enforces continuity upon the deformed grown state. The growth component is driven by the concentration of a single chemical, c, and moderated by the mean mechanical stress (hydrostatic pressure), p, at the tumour-ECM boundary:

$$E^g = \begin{cases} \dfrac{g(t)c}{c+k}(1-\dfrac{p}{B}), & \text{if } p \leq B \\ 0, & \text{if } p > B \end{cases} \tag{1}$$

Where E^g is the nominal Green strain due to growth, c is the concentration of oxygen, $g(t)$ is a Gompertzian function of time described in Section 4.2, and k and B are constants taken from the literature (Kim et al, 2011). Here we enforce $0 \leq p \leq B$, such that growth approaches zero as $p \to B$. The expression assumes a Michaelis-Menten form, which is a physically-derived model for enzyme kinetics which has been shown to apply to tumour cell oxygen consumption (Casciari et al, 1992). Here we assume that the concentration of oxygen is constant across the domain, with the nutrient-dependent limit on tumour size captured by the experimentally derived variable $g(t)$. The deformation gradient due to growth is then returned by first calculating the corresponding volumetric stretch, λ (Malvern, 1977):

$$\lambda = \sqrt{2E^g + 1} \tag{2}$$

Hence, assuming isotropic cancer mass growth (Ambrosi and Mollica, 2002; Lubarda and Hoger, 2002):

$$F^g_{ij} = \lambda\delta_{ij} \tag{3}$$

Finally, the mechanical strains of the tissues are calculated from the constitutive equation provided by the elastic deformation gradient tensor, F^p_{ij}:

$$F^p_{ij} = F_{ik}(F^g_{kj})^{-1} \tag{4}$$

To enable an anisotropic description of tumour growth, Equation 3 can be adapted to include off-diagonal elements. However, a simple growth model is utilised as the focus of this work is on the multiscale response of the ECM to growth-induced stress, and how ECM microstructure influences tumour morphology.

2.2 Macroscopic problem

The conservation of linear momentum in a continuum, assuming zero inertia, is expressed as:

$$S_{ij,i} - Q_j = 0 \tag{5}$$

Where S_{ij} is the 2nd Piola-Kirchoff stress tensor and Q_j represents body forces and source terms. Viscous effects are ignored due to the small growth rate under consideration: an approximately 3 mm increase in radius per week. Making use of the principle of virtual work, the weak form of the balance equation reads (Hughes, 2000):

$$-\int_\omega \delta u_{i,j} S_{ij} dV + \int_{\partial\omega} \delta u_i S_{ij} N_j dS + \int_\omega \delta u_j Q_j dV = 0 \tag{6}$$

Where δu_i is a virtual displacement, N_i is the outward boundary normal and Q_j is a source term in domain ω. The second term vanishes if the boundary, $\partial\omega$,

is assumed traction-free. This equation can then be discretised using the Galerkin finite element (FE) method, using Lagrange polynomials as basis functions (Bathe, 1996). Depending on the domain, the constitutive behaviour is determined by either a compressible hyperelastic continuum, a microscopic volume averaged continuum, or a combination of both. In the foremost case, the 2nd Piola-Kirchoff stress is given by (Malvern, 1977):

$$S_{ij} = 2\,\frac{\partial W}{\partial C^p_{ij}} \tag{7}$$

Where C^p_{ij} is the right Green-Cauchy "passive" deformation tensor. For all macroscopic tissues, the following strain-energy density function has been adopted: $W = \mu/2\,(I_1-3)+K/2\,(J-1)^2$, where for small deformations the material coefficients μ and K correspond to the shear and bulk modulus, respectively, while I_1 is the trace of C^p_{ij}, $I_1 = tr(F^p_{ki}F^p_{kj})$, and J is the determinant of F^p_{ij}.

2.3 Microscopic problem

Following (Stylianopoulos and Barocas, 2007), collagen networks are modelled using the representative volume element (RVE) concept. An RVE is defined as being the smallest possible unit that is representative of the heterogeneous material under the assumption of statistical homogeneity (Hori and Nemat-Nasser, 1999). As shown in Figure 2, each RVE is centred on the Gauss integration points of the macroscopic FE.

Network generation proceeds like collagen fibrillogenesis (Veis, 1982): first, a random distribution of nodes is defined within a cube. At each node two lines are incremented outwards along random vectors in opposite directions; upon meeting another line or the boundary, another node is created and line expansion stops. Networks can also be created with a preferred initial orientation by rotating the nodes about the origin according to an input prior rotation matrix, with the process iterated until the RVE averaged orientation tensor falls within a given tolerance of the prior.

This specifies a scaffold of one-dimensional truss elements connected at nodes, allowing for translations and rotations. The microscopic boundary value problem is then posed by interpolating the macroscopic nodal displacements to the RVE boundary nodes. This process is explained in more detail in Section 4.

Following the work of (Chandran and Barocas, 2007), we require the resulting residual forces on internal nodes, r_i, to be zero:

$$r_i = \sum f_i \tag{8}$$

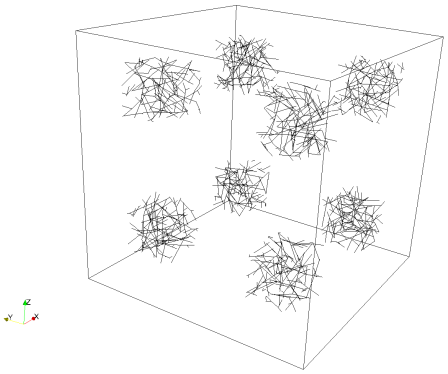

Fig. 2: Example hexahedral FE with RVEs centred at its quadrature points. The RVEs are scaled up for visual purposes.

Where summation is over every fibre sharing the same node, and f_i is the force due to the $n-$th fibre acting on the node. The fibre constitutive equation assumes an exponential form (Billiar and Sacks, 2000b), which reflects experimental observations that fibres are initially in a slack rest-state then rapidly stiffen under uniaxial extension (Billiar and Sacks, 2000a). Furthermore, a negative phase is included to account for fibre buckling; that is, near-zero negative stress under compression:

$$f_i = \alpha(e^{\beta E} - 1)n^f_i \tag{9}$$

Here f_i is the force along the fibre, α and β are constants, E is the Green-Lagrange strain and n^f_i is the fibre unit vector. Specifically, $\alpha = \frac{E_f A_f}{\beta}$, where E_f is the fibre elastic modulus, A_f the fibre cross-sectional area and β a dimensionless nonlinearity parameter. As such α can be thought of as defining the magnitude of the force response, which can be derived from experimental data.

2.4 Scale coupling

Volume averaging theory is used to couple the micro and macroscopic scales (Hori and Nemat-Nasser, 1999). Based on the principle that measured effective properties are averages of heterogeneous microscopic fields, it defines macroscopic fields as volume averages of their microscopic counterpart. Accordingly, the macroscopic stress, S_{ij}, can be expressed in terms of the microscopic stress tensor at the RVE surface, s_{ij}, as:

$$S_{ij} = \frac{1}{V}\int_\xi s_{ij}dV \tag{10}$$

Where V is the volume of the RVE and the integral is over the RVE surface, ξ. The microscale stress tensor

is expressed in terms of the fibre force on the boundary:

$$s_{ij} = n_i^f n_j^b |f| \tag{11}$$

Where n_i^f is the fibre unit vector, n_j^b is the outward unit vector at the intersection point of a fibre with the RVE boundary, $\partial\omega$, and f is given by Equation 9. Assuming microscopic equilibrium and via the application of the divergence theorem, Equation 10 can be redefined in terms of the RVE boundary node position, x_i, and net force, f_i, in a discrete manner as:

$$S_{ij} = \frac{1}{V} \sum x_i f_j \tag{12}$$

Where the sum is over RVE boundary nodes. Again following (Chandran and Barocas, 2007), the macroscopic source term, Q_j, can be expressed in terms of the difference between the micro- and macroscopic stress, respectively, as:

$$Q_j = \frac{1}{V} \int_{\partial\omega} (s_{ij} - S_{ij}) u_{k,i} n_k dS \tag{13}$$

Here u_i is the RVE boundary displacement and n_k is the outward unit normal vector to $\partial\omega$. This term arises from the correlation between RVE boundary node displacements and the macroscale stress field (see (Chandran and Barocas, 2007) for details of the derivation). This representation establishes a boundary value problem with conditions defined at the macroscopic scale.

For the average to be a meaningful representation of local material behaviour, it is necessary for the size of the RVE to be larger than the volume over which the microfield gradient varies but smaller than the corresponding volume over which the macrofield gradient varies (Chandran and Barocas, 2007). This is ensured here by employing a material RVE with boundary deformation prescribed by interpolating the macroscopic displacement field. As such, the distances over which fibre interactions are correlated can become large enough to preclude a homogeneous macroscopic deformation.

As a final comment, volume averaging theory was chosen over homogenisation theory due to its relative ease of application. While homogenisation theory provides higher order calculations, to first order the two theories are approximately equivalent (Hori and Nemat-Nasser, 1999). Given that this analysis does not require precision calculations, volume averaging theory is an appropriate choice.

In order to simplify the numerical procedure (discussed in the following section), RVEs are defined in the FE parametric space. Therefore, to map between the parametric space — where calculations at the microscale are performed — and physical space — where calculations at the macroscale are performed — it is necessary to define the Jacobian, J, of the transform, $S'_{ij} = JS_{ij}$, where the prime indicates a physical stress:

$$J = \frac{\theta_0 V^{\mathrm{RVE}}}{L A_f} \tag{14}$$

As per (Stylianopoulos and Barocas, 2007), we express the Jacobian in terms of the collagen volume fraction in the RVE, θ_0, the RVE parametric volume, V^{RVE}, the total parametric fibre length in the RVE, L, and the physical collagen fibre cross-sectional area, A_f. Note that S_{ij} initially has units of force due to the fibre constitutive equation (Equation 9). The same transformation is performed to dimensionalise the source term, Q_j.

3 Experimental procedure

To bestow the simulations with biologically representative material and kinematic parameters, data from studies of mouse tumour growth were utilised. Details of how these data were acquired are given in the following sections.

3.1 Cell culture and in vivo models

The human breast cancer cell line MCF10CA1a, derived from *in vivo* passaging of H-Ras transformed MCF10A cells (Santner et al, 2001) was used in the current study. Cells were cultured in DMEM F/12 medium supplemented with 5% horse serum, 10 µg/ml insulin, 20 ng/ml EGF, 0.1 µg/ml hydrocortisone and 0.5 µg/ml cholera toxin (Papageorgis et al, 2010) and were maintained under standard conditions (37°C, 5% CO_2 and 95% humidity) until 75-80% confluent. Cultures were then trypsinised, washed twice and resuspended in serum-free media. Tumours were prepared by implanting 0.5-1.0 million MCF10CA1a cells suspended in 100 µl serum-free media into the third mammary fat pad of immunodeficient 6-week old CD1 nude female mice.

Tumour growth was monitored and its planar dimensions (x, y) were measured with a digital caliper. Tumour volume was measured from the planar dimensions using the volume of an ellipsoid and assuming that the third dimension, z, is equal to $\sqrt{xy}$ (Voutouri et al, 2014). Therefore, the volume was given by the equation: $V = \frac{4\pi}{3}\frac{xyz}{8}$, which yields $V = \frac{\pi\sqrt{xy}^{3/2}}{6}$. When tumours reached approximately 10 mm (520 mm^3) in size, mice were sacrificed via NO inhalation and tumours were excised for the mechanical characterisation measurement. Eight animals/tumours were used (n = 8). The experiments were conducted in strict accordance with the

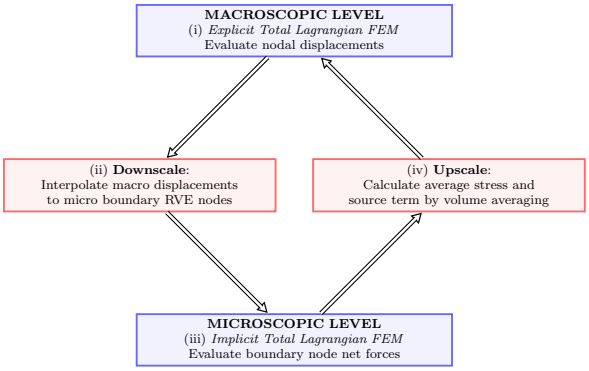

Fig. 3: Multiscale algorithm structure.

animal welfare regulations and guidelines of the Republic of Cyprus and the European Union under a license acquired by the Cyprus Veterinary Services (No CY/EXP/PR.L1/2014), the Cyprus national authority for monitoring animal research.

3.2 Mechanical testing of tumour specimens

Stress relaxation experiments under unconfined compression were performed in tumour specimens to measure the mechanical response of the tissues. An Instron high precision mechanical testing system was used (Instron 5944, Norwood, MA). Following tumour excision, the specimens were cut in orthogonal shapes with approximate dimension 5 × 5 × 3 mm (length × width × thickness) and placed between two parallel platens. The experimental protocol consisting of four cycles of 5% compression of 1 minute duration followed by a 10 minute hold, which was determined sufficient time for the transient, poroelastic response of the material to vanish and the equilibrium stress at each strain interval to be recorded. The 1st Piola-Kirchhoff stress was calculated by dividing the measured force by the initial cross sectional area of the specimen. Stress-strain curves were constructed by plotting the equilibrium stress as a function of strain.

4 Numerical methodology

4.1 Algorithm

The algorithmic structure is presented in Figure 3 and performed as follows:

1. At the first stage the macroscopic boundary value problem is posed and solved via an explicit Total Lagrangian finite element method (FEM) solver. The outer surfaces of the macroscopic domain are prescribed as having zero displacement, $u_i = 0$.
2. The resulting displacement field is interpolated from the macroscopic FE nodes to the RVE boundary nodes ("downscaled") via:
$$u_i = \sum U_i \phi \tag{15}$$
Here u_i is the $n-$th RVE boundary node displacement, U_i is the $N-$th FE node displacement and ϕ is the corresponding interpolation function. Since the RVE is defined in the FE parametric space, only a single mapping between it and the physical space is necessary.
3. With the node displacements prescribed on the RVE boundary, the microscopic boundary value problem is posed (Equation 8) and solved using a fully-implicit Total Lagrangian FEM. To ensure numerical stability of the algorithm, a damped Newton-Raphson scheme is implemented. Specifically, a diagonal matrix, with magnitude iteratively optimised to the necessary degree of damping, is added to the tangent stiffness matrix. The resulting internal node displacements are then used to evaluate the net force on the boundary nodes (Equation 9) and hence the microscale stress field, s_{ij} (Equation 11).
4. Finally, the macroscale stress (Equation 12) and source term (Equation 13) are calculated from the microscale stress field by volume averaging theory. The computed fields are then used to assemble the internal force and source terms of the unbalanced forces' *rhs* vector. The explicit system is solved and the solution is advanced in time.

The above procedure is repeated until termination of the tumour growth.

The algorithm was implemented in C++ in an open-source, parallelised finite element solver framework developed by the authors[1], which incorporates various open-source scientific computing libraries: libMesh (Kirk et al, 2006), PETSc (Balay et al, 1997), blitz++, GSL and MPICH.

4.2 Material Parameters

The material parameters presented in Table 1 are used in all simulations unless stated otherwise. Growth parameter $g(t)$ is given by a Gompertz-type function of the form: $g(t) = a\exp(-b\exp(-\gamma t))$, fitted to data (Figure 4) from the *in vivo* mouse tumour studies described previously. In order to render $g(t)$ dimensionless, parameter a is normalised. Data from the same experiments were used to determine the tumour material

[1] FEB3: Finite Element Bioengineering in 3D, publicly available from https://bitbucket.org/vasvav/feb3-finite-element-bioengineering-in-3d

Table 1: Material parameters used in simulations.

Parameter	Description	Value	Source
a	Growth rate parameter	1.0	This work
b	Growth rate parameter	12.8	This work
γ	Growth rate parameter	0.126 day^{-1}	This work
k	Growth rate parameter	8.3 $\times 10^{-3}$mol/m^3	(Casciari et al, 1992)
B	Stress feedback term	11 kPa	(Kim et al, 2011)
c	O_2 concentration	0.2 mol/m^3	(Kim et al, 2011)
μ_T	Tumour shear modulus	1.45 kPa	This work
K_T	Tumour bulk modulus	14.01 kPa	This work
μ_{ECM}	ECM shear modulus	1.42 kPa	This work
K_{ECM}	ECM bulk modulus	3.08 kPa	This work
E_f	Fibre elastic modulus	10 MPa	(Silver et al, 2001)
A_f	Fibre cross-sectional area	1963 nm^2	(Stylianopoulos and Barocas, 2007)
β	Fibre nonlinearity parameter	1.0	(Stylianopoulos and Barocas, 2007)
θ_0	RVE fibre volume fraction	0.3	(Stylianopoulos and Barocas, 2007)
V^{RVE}	RVE volume	0.076	This work
L	RVE total fibre length	[15,21]	This work

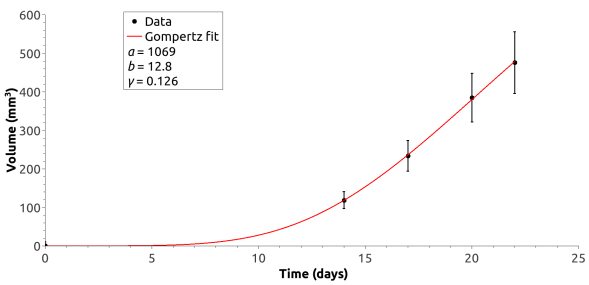

Fig. 4: Mouse tumour volume as a function of time. Standard errors and fit coefficients are provided.

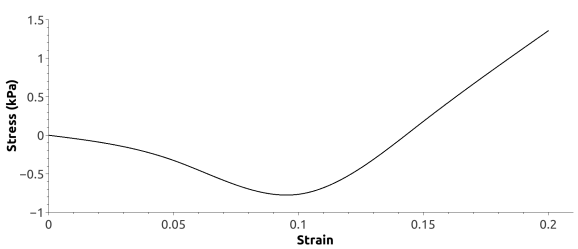

Fig. 5: Example mouse tumour stress-strain graph.

properties, assuming a Poisson's ratio of $\nu = 0.45$; an example stress-strain graph is shown in Figure 5. The collagen material properties were set to a typical order of magnitude for type I collagen under small strain. The ECM material properties were chosen to produce a similar elastic modulus as an 2 mg/ml agarose gel comprised of type I collagen.

RVE volume, V^{RVE}, and total fibre length, L, are determined at the pre-processing stage, when RVE network generation is executed. The volume is chosen such that the RVE, which is centred on a quadrature point, remains within the FE parametric space, [-1,1]. As such, it depends on the quadrature rule used to perform the integration: all calculations presented here use an eight-point Gauss-Legendre quadrature rule. Since networks were randomly generated, the total fibre length and number of fibres varied between RVEs and simulations:

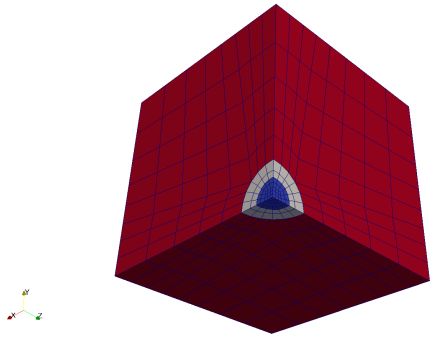

Fig. 6: FE mesh with domains corresponding to Figure 1; from centre out: tumour, PTS and ECM. The radius of the tumour is 0.1mm, the thickness of the PTS is 0.15mm, and the thickness of the ECM is 1.25mm.

the former from approximately 200-300 and the latter from 15-21.

The FE mesh used in all simulations is shown in Figure 6 and represents an octant comprised of 620 hexahedral elements, with a total of 877 nodes. All simulations were performed on a single 1.2 MHz desktop machine with 16 CPUs operating Linux, with a wall time of less than 10 minutes for the affine simulations and approximately 24 hours for the non-affine simulations. The difference between these cases is described in the following section.

5 Results

5.1 Affine versus non-affine models

To justify the theoretical and computational expense of employing a multiscale model, Figure 7 compares the stress-stretch relationships as a result of tumour growth for non-affine and affine network modelling of the elements at the tumour-PTS boundary. Here we define (non-)affine as the (non-)affine displacement of the internal RVE nodes with respect to the macroscale gradient. Therefore in the affine model no force balance is solved at the microscale; instead, the macroscopic nodal displacement is interpolated to every node in the RVE according to Equation 15. This results in each fibre deforming in a manner continuous with the macroscopic deformation. As such this modelling approach is equivalent to a conventional continuum model with an anisotropic fibre component (see for example Kroon and Holzapfel 2008), with the fibres unable to rearrange at their cross-links to minimise the stress. This is reflected in the affine model displaying a larger negative stress than the non-affine model, an observation that is in accordance with comparisons of network kinematics

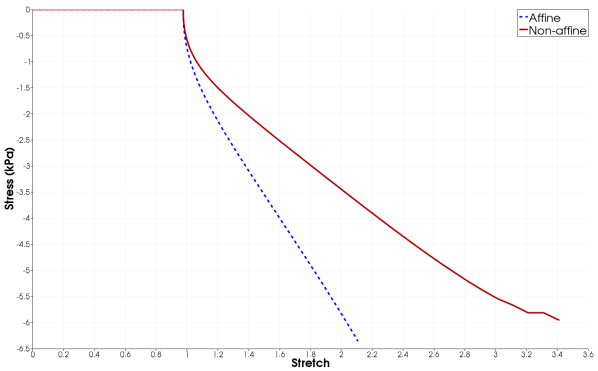

Fig. 7: Principal stress versus principal stretch for affine and non-affine network models.

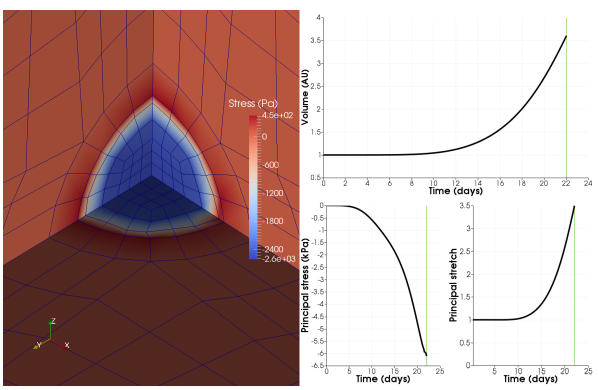

Fig. 8: Clockwise from left: final state solid stress and deformation due to tumour growth into a multiscale PTS and a continuum ECM; tumour volume against time; tumour principal stretch against time; tumour principal stress against time.

performed by (Chandran and Barocas, 2006). Furthermore, the non-affine model permits a larger maximum tumour volume; this can be reasoned in terms of network rearrangement accommodating for the compressive stress to find a minimum residual. The kink in the tail of the non-affine graph is due to some of the RVE networks collapsing, and is discussed in the next section.

5.2 Effect of tumour growth on peritumoural microstructure

To investigate the effect of tumour growth on peritumoural microstructure, the tumour was allowed to grow to over 3 times its initial volume. The final state mesh deformation, solid stress distribution and graphs of the tumour growth and principal stress against principal stretch are shown in Figure 8. The tumour experiences a compressive pressure from the PTS and ECM, as expected. Growth follows the prescribed Gompertz function, with a corresponding increase in the tumour principal stretch. The principal stress increases negatively, but begins to increase positively near the maximum time. This is due to elements adjacent to the tumour boundary being either almost or completely collapsed by the growth. At the microscale this effect is explained by the networks inside the elements being unable to support large compression, as shown in Figure 9: networks close to the boundary collapse, while those in the next layer can support the compression.

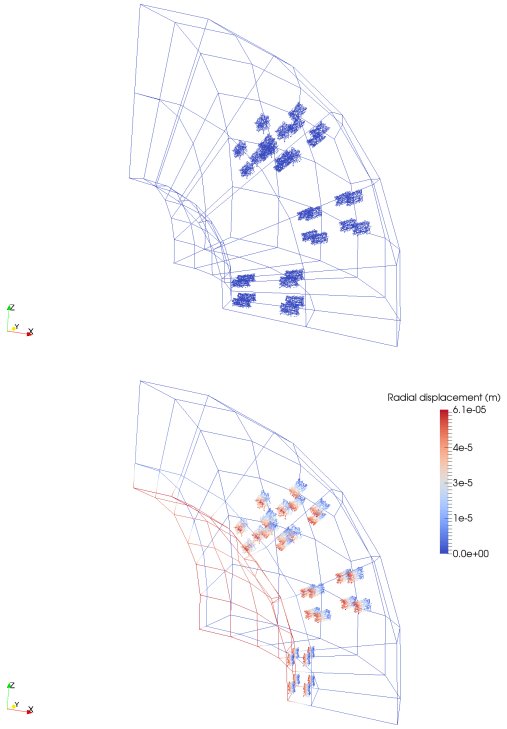

Fig. 9: PTS domain. Simulated initial (top) and final (bottom) RVE network deformation. The radial displacement is given at the macroscopic scale.

Examining the microscale further, Figure 10 shows the principal eigenvector of each averaged RVE orientation tensor, Ω_i, defined as (Barocas and Tranquillo, 1997):

$$\Omega_i = \frac{\sum l_i^2/l}{\sum l} \tag{16}$$

Where l_i is the projection of fibre n of length l in the $i-$direction, and the sum is over all fibres in the RVE. As quantified in the histograms, the networks have an initially random alignment with respect to the tumour boundary. In the final state the networks nearest the boundary realign to a parallel orientation, representing a passive mechanical response to tumour growth (see Jackson and Byrne 2002). This qualitatively re-

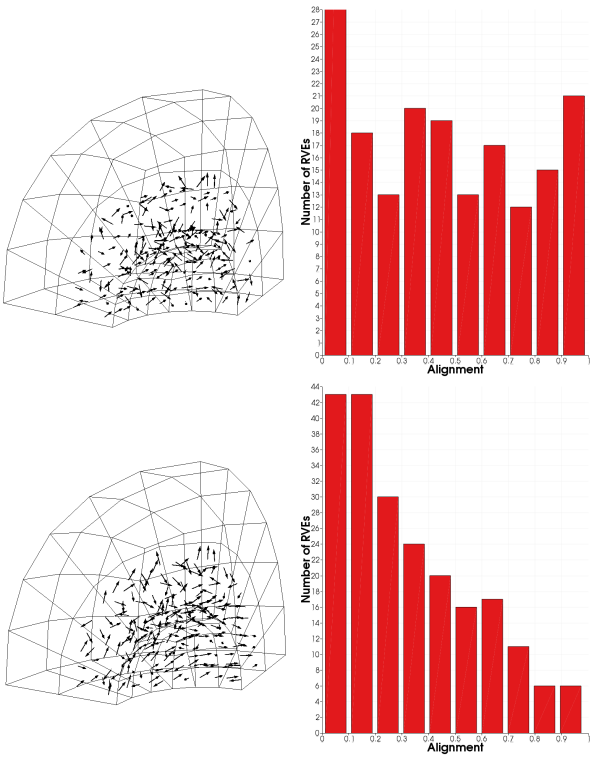

Fig. 10: RVE network alignment for elements at the tumour-PTS boundary in the initial (top) and final (bottom) states. A value of 1 indicates radial alignment; a value of 0 indicates circumferential alignment.

produces part of the *in vitro* observations made by (Provenzano et al, 2006).

To examine the effect of peritumoural microstructure on tumour morphology, the final state tumour dimensions were examined for two types of initial peritumoural collagen alignment: random and aligned in the $z-$direction. In both cases the tumour grew approximately 5% more in a single direction (z for the aligned case). This demonstrated a dependency of tumour morphology on initial network orientation: if a given network was arranged with a strong radial component, more fibres were aligned with the axis of compression and hence buckled as the tumour expanded. It is interesting to note that the same simulations performed with an affine fibre deformation produced anisotropy at the 10% level in the aligned case and approximately 7% in the random case. Comparing the final fibre alignment distributions for the two deformation types showed that this effect was due to the non-affine deformation permitting internal fibre reorientation, and hence a reduced dependency on the initial orientation.

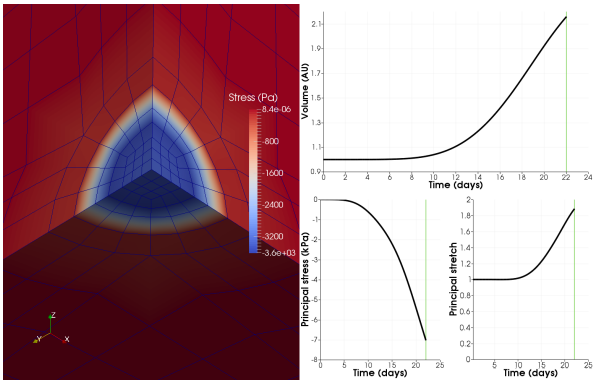

Fig. 11: Clockwise from left: final state solid stress and deformation due to tumour growth into a multiscale, two-component PTS and a continuum ECM; tumour volume against time; tumour principal stretch against time; tumour principal stress against time.

5.3 Two-component model

The preceding model demonstrated the influence of collagen networks in tumour-stroma interactions, where peritumoural tissue is modelled as a scaffold of collagen fibres. However, this is not biologically representative; *in vivo*, the collagen is embedded in a non-collagenous matrix. To reflect this an additional component, treated as a hyperelastic solid, was added to the PTS constitutive equation. Hence, S_{ij} is computed as the superposition of the collagen derived mechanical stresses inherent from the microstructure (Equation 12) and the biomechanical response of the stroma matrix (Equation 7). The material parameters were set equal to those of the ECM and the simulation was performed with exactly the same growth function as in the previous section. As can be seen in Figure 11, the resulting deformation is reduced, giving a more symmetric expansion of the cancer region. Furthermore, the final state volume and principal stretch are reduced. As a result, network reorientation was observed but to a lesser degree than the single component model.

6 Conclusions

In this paper we have presented a computational model of solid tumour growth coupled with a multiscale biomechanical description of the tumour periphery. The mathematical formulation facilitates the explicit calculation of fibre-fibre and tumour-fibre interactions, enabling the relationship between growth and microstructural remodelling to be examined. The aim was to demonstrate that such a model, which considers only mechanical interactions, could be used to explain experimental

observations of the effects of solid tumour growth on its microenvironment and vice versa.

Data-driven growth simulations were performed and compared to experimental observations. As an initial proof-of-concept, affine and non-affine network models were compared. The resulting stress-stretch relationship qualitatively reproduced previous findings (Chandran and Barocas, 2006), indicating that a non-affine approach is necessary to capture the internal reorganisation of collagen networks under strain.

The model qualitatively replicates the passive reorientation of collagen fibres at the tumour-ECM interface from a random to parallel alignment with respect to the tumour boundary (Provenzano et al, 2006). This confirms the hypothesis that this process can be explained purely in terms of near-field collagen network compression.

The effect of initial network orientation on tumour morphology was also investigated, with simulations indicating that an anisotropic distribution of networks produces anisotropic growth at the 5% level. This dependency was found to be reduced when an additional component — representing the non-fibrous part of the stroma — was added to the biomechanical model of the peritumoural stroma. As such, we propose that it is the non-collagenous component that permits non-load-bearing (ie. perpendicular) collagen alignments at the tumour boundary.

The model described here has many simplifications with respect to *in vivo* conditions, to name a few: only solid mechanics is considered, growth is described by the uptake of a single nutrient, and there are no stromal cells that remodel the intra-tumour collagen fibres (eg. fibroblasts). Another simplification is the domain dependent application of the multiscale model. However, this can be justified when considering that collagen remodelling was shown to occur predominantly in the first layer of elements adjacent to the tumour. Furthermore, given that the stresses inside the tumour are compressive, during growth the collagen networks would collapse and there would be little benefit in modelling inter-tumour fibre interactions.

Acknowledgements The authors from UCL would like to thank Dr. Rebecca Shipley (UCL IBME) for many useful discussions. The authors from UCL received funding from EPSRC grant "MIMIC": EP/K020439/1, EU FP7 Virtual Physiological Human grant: "VPH-PRISM" (FP7-ICT-2011-9, 601040) and Marie-Curie Fellowship (FP7-PEOPLE-2013-IEF, 627025). The authors from UCY received funding from the European Research Council (FP7/2007-2013)/ERC Grant No. 336839-ReEngineeringCancer.

References

Ambrosi D, Mollica F (2002) On the mechanics of a growing tumor. International Journal of Engineering Science 40:1297–1316

Ambrosi D, Mollica F (2004) The role of stress in the growth of a multicell spheroid. Journal of Mathematical Biology 48:477–499

Ambrosi D, Preziosi L (2009) Cell adhesion mechanisms and stress relaxation in the mechanics of tumours. Biomechanics and Modeling in Mechanobiology 8:397–413

Balay S, Gropp WD, McInnes LC, Smith BF (1997) Efficient management of parallelism in object oriented numerical software libraries. In: Arge E, Bruaset AM, Langtangen HP (eds) Modern Software Tools in Scientific Computing, Birkhäuser Press, pp 163–202

Barocas V, Tranquillo R (1997) An anisotropic biphasic theory of tissue-equivalent mechanics: the interplay among cell traction, fibrillar network deformation, fibril alignment, and cell contact guidance. J Biomech Engrg 119:137–145

Bathe KJ (1996) Finite element procedures. USA: Prentice Hall p 456

Billiar KL, Sacks MS (2000a) Biaxial mechanical properties of the native and glutaraldehyde-treated aortic valve cusp: Part i: Experimental results. J Biomech Engrg 122:23–30

Billiar KL, Sacks MS (2000b) Biaxial mechanical properties of the native and glutaraldehyde-treated aortic valve cusp: Part ii - a structural constitutive model. J Biomech Engrg 122:327–335

Butcher DT, Alliston T, Weaver V (2009) A tense situation: forcing tumour progression. Nature 9:108–122

Byrne H (2010) Dissecting cancer through mathematics: from the cell to the animal model. Nature Reviews Cancer 10:221–230

Casciari J, Sotirchos S, Sutherland R (1992) Variations in tumor cell growth rates and metabolism with oxygen concentration, glucose concentration, and extracellular ph. J Cell Physiol 151:386–394

Chandran PL, Barocas VH (2006) Affine versus non-affine fibril kinematics in collagen networks: Theoretical studies of network behavior. Journal of Biomechanical Engineering 128:259–270

Chandran PL, Barocas VH (2007) Deterministic material-based averaging theory model of collagen gel micromechanics. J Biomech Engrg 129:137–147

Chen CS, Mrksich M, Huang S, Whitesides GM, Ingber DE (1997) Geometric control of cell life and death. Science 276:1425–1428

Cheng G, Tse J, Jain RK, Munn LL (2009) Micro-environmental mechanical stress controls tumor

spheroid size and morphology by suppressing proliferation and inducing apoptosis in cancer cells. PLoS ONE 4

Conklin MW, Keely PJ (2012) Why the stroma matters in breast cancer. Cell Adhesion and Migration 6:249–260

Cristini V, Lowengrub J (2010) Multiscale Modeling of Cancer: An Integrated Experimental and Mathematical Modeling Approach, 1st edn. Cambridge University Press, The Edinburgh Building, Cambridge CB2 8RU, UK, chapter 1 and 3

Discher DE, Janmey P, Wang YL (2005) Tissue cells feel and respond to the stiffness of their substrate. Science 310:1139–1143

Frieboes H, Chaplain M, Thompson A, Bearer E, Lowengrub J, Cristini V (2011) Physical oncology: a bench-to-bedside quantitative and predictive approach. Cancer Research 71:298–302

Helmlinger G, Netti PA, Lichtenbeld HC, Melder RJ, Jain RK (1997) Solid stress inhibits the growth of multicellular tumor spheroids. Nature Biotechnology 15:778–783

Hori M, Nemat-Nasser S (1999) On two micromechanics theories for determining micro-macro relations in heterogeneous solids. Mechanics of Materials 31:667–682

Hughes TJR (2000) The Finite Element Method: Linear Static and Dynamic Finite Element Analysis, 1st edn. Dover Publications

Jackson TL, Byrne H (2002) A mechanical model of tumor encapsulation and transcapsular spread. Mathematical Biosciences 180:307–328

Jain RK, Martin JD, Stylianopoulos T (2014) The role of mechanical forces in tumor progression and therapy. Ann Rev Biomed Eng 16:321–346

Janmey PA (1998) The cytoskeleton and cell signaling: Component localization and mechanical coupling. Physiological Reviews 78:763–781

Kam Y, Rejniak K, Anderson A (2012) Cellular modeling of cancer invasion: integration of in silico and in vitro approaches. Journal of Cell Physiology 227:431–438

Kim Y, Stolarska MA, Othmer HG (2011) The role of the microenvironment in tumor growth and invasion. Progress in Biophysics and Molecular Biology 106:353–379

Kirk BS, Peterson JW, Stogner RH, Carey GF (2006) `libMesh`: A C++ Library for Parallel Adaptive Mesh Refinement/Coarsening Simulations. Engineering with Computers 22(3–4):237–254

Kroon M, Holzapfel GA (2008) A new constitutive model for multi-layered collagenous tissues. Journal of Biomechanics 41:2766–2771

Liotta LA, Kohn EC (2001) The microenvironment of the tumour-host interface. Nature 411:375–379

Lubarda VA, Hoger A (2002) On the mechanics of solids with a growing mass. International Journal of Solids and Structures 39:4627–4664

Malvern LE (1977) Introduction to the Mechanics of a Continuous Medium, 1st edn. Prentice Hall

Mpekris F, Angeli S, Pirentis A, Stylianopoulos T (2015) Stress-mediated progression of solid tumors: effect of mechanical stress on tissue oxygenation, cancer cell proliferation, and drug delivery. Biomech Model Mechanobiol URL http://www.ncbi.nlm.nih.gov/pubmed/25968141

Netti PA, Berk DA, Swartz MA, Grodzinsky AJ, Jain RK (2000) Role of extracellular matrix assembly in interstitial transport in solid tumors. Cancer Research 60:2497–2503

Papageorgis P, Lambert A, Ozturk S, Gao F, Pan H, Manne U, Alekseyev Y, Thiagalingam A, Abdolmaleky H, Lenburg M, Thiagalingam S (2010) Smad signaling is required to maintain epigenetic silencing during breast cancer progression. Cancer Research 70:1916–1930

Paszek MJ, Zahir N, Johnson KR, Lakins JN, Rozenberg GI, Gefen A, Reinhart-King CA, Margulies SS, Dembo M, Boettiger D, Hammer DA, Weaver VM (2005) Tensional homeostasis and the malignant phenotype. Cancer Cell 8:241–254

Pelham RJ, Wang YL (1997) Cell locomotion and focal adhesions are regulated by substrate flexibility. PNAS 94:13,661–13,665

Preziosi L, Ambrosi D, Verdier C (2010) An elasto-visco-plastic model of cell aggregates. Journal of Theoretical Biology 262:35–47

Provenzano PP, Eliceiri KW, Campbell JM, Inman DR, White JG, Keely PJ (2006) Collagen reorganization at the tumor-stromal interface facilitates local invasion. BMC Medicine 4:38

Rodriguez EK, Hoger A, McCulloch AD (1994) Stress-dependent finite growth in soft elastic tissues. J Biomechanics 27:455–467

Santner SJ, Dawson PJ, Tait L, Soule HD, Eliason J, Mohamed AN, Wolman SR, Heppner GH, Miller FR (2001) Malignant mcf10ca1 cell lines derived from premalignant human breast epithelial mcf10at cells. Breast Cancer Research and Treatment 65:101–110

Silver FH, Horvath I, Foran DJ (2001) Viscoelasticity of the vessel wall: the role of collagen and elastin fibers. Crit Rev Biomed Engrg 29:279–301

Stylianopoulos T, Barocas VH (2007) Volume-averaging theory for the study of the mechanics of collagen networks. Comput Methods Appl Mech Engrg 196:2981–2990

Stylianopoulos T, Martin JD, Chauhan VP, Jain SR, Diop-Frimpong B, Bardeesy N, Smith BL, Ferrone CR, Hornicek FJ, Boucher Y, Munn LL, Jain RK (2012) Causes, consequences, and remedies for growth-induced solid stress in murine and human tumors. PNAS 109:15,101–15,108

Stylianopoulos T, Martin JD, Snuderi M, Mpekris F, Jain SR, Jain RK (2013) Coevolution of solid stress and interstitial fluid pressure in tumors during progression: Implications for vascular collapse. Cancer Research 73:3833–3841

Veis A (1982) Collagen fibrillogenesis. Connect Tissue Res 10:11–24

Voutouri C, Mpekris F, Papageorgis P, Odysseos AD, Stylianopoulos T (2014) Role of constitutive behavior and tumor-host mechanical interactions in the state of stress and growth of solid tumors. PLoS One 9:e104,717

Yeung T, Georges PC, Flanagan LA, Marg B, Ortiz M, Funaki M, Zahir N, Ming W, Weaver V, Janmey PA (2005) Effects of substrate stiffness on cell morphology, cytoskeletal structure and adhesion. Cell Motility and the Cytoskeleton 60:24–34